Neoclassical Transport in the Helical Reversed-Field Pinch

M. Gobbin,[1,*] G. Spizzo,[1,†] L. Marrelli,[1] and R. B. White[2]

[1]Consorzio RFX, Euratom-ENEA Association, Corso Stati Uniti, 4 35127 Padova-Italy

[2]Plasma Physics Laboratory, Princeton University, P.O. Box 451, Princeton, New Jersey 08543 USA

(Received 7 June 2010; published 4 November 2010)

Test particle evaluation of the diffusion coefficient in a fusion plasma in the reversed-field pinch (RFP) configuration shows distinct similarities with stellarators when the plasma spontaneously evolves towards a helical shape. The almost total absence of superbanana particles at the levels of helical deformation seen in experiment ($B_h/B = 10\%$) causes transport to be proportional to collision frequency (at low collisions). This fact excludes the possibility that the minimum conceivable transport could be inversely proportional to collision frequency, which is typical of unoptimized stellarators. This result strengthens the perspectives of the helical RFP as a fusion configuration.

DOI: 10.1103/PhysRevLett.105.195006 PACS numbers: 52.20.Dq, 05.40.Fb, 52.55.Hc, 52.65.Cc

In plasmas, binary Coulomb collision frequency scales with temperature as $\sim T^{-3/2}$. Thus, evaluating regimes of transport as a function of collision frequency is fundamental in any study of a fusion reactor based on magnetic confinement, as for example, those performed for ITER [1].

In the tokamak and stellarator the neoclassical diffusion coefficient as a function of collisionality traverses three regimes, namely, banana (BN), plateau (PL) and Pfirsch-Schlüter (PS) regimes (see, e.g., Refs. [2,3]). The same study for the reversed-field pinch (RFP), a configuration for plasma confinement characterized by the reversal of the safety factor $q = d\psi/d\psi_p$ at the edge (ψ, ψ_p being the toroidal and poloidal magnetic fluxes, respectively), has been performed in axisymmetric geometry only [4]. Moreover, when in the RFP state called multiple helicity (MH) magnetic chaos exceeds neoclassical effects, the Rechester-Rosenbluth paradigm asserts that collisions should reduce the effect of magnetic chaos in spreading particle orbits [5]. More recently, it has been shown that, for small Kubo numbers [6], collisions allow decorrelations of particles from the magnetic field lines and determine a transition of stochastic transport from the quasilinear, to the subdiffusive and Rechester-Rosenbluth regimes. Higher Kubo numbers correspond to the percolative regime where strong anisotropy is to be expected [7].

Contrary to the MH, in the ordered helical QSH (quasi-single helicity) state [8,9] one may expect the tokamak-stellarator scaling to be valid due to the significant reduction of magnetic chaos. This state has been achieved experimentally in the reversed-field experiment (RFX-mod) [10], by increasing the plasma current up to $\sim$1.5 MA [11].

In this Letter we will describe the regimes of transport as a function of collision frequency in MH and QSH. Presently we limit our discussion to magnetic turbulence due to global tearing instabilities: the results in QSH are therefore a theoretical description of the perspectives of the RFP configuration in the limit of no microturbulence. With this caveat, we will show that in QSH the RFP shows the usual three regimes of neoclassical transport, while in MH the banana regime is superseded by the chaotic transport. Since QSH is strongly helical symmetric, one could speculate that the role of the so-called helically trapped (''superbanana'') particles should be prominent, in the same way as in most unoptimized stellarators [12,13]. But we will show that this is not the case, since for the amplitude of the helical deformation typical of the QSH ($B_h/B_{0,0} \sim 10\%$) the helical ripple at the edge is still small, with no big ripple-induced superbanana losses (B_h and $B_{0,0}$ are the helical and axisymmetric components of the magnetic field). Superbananas become evident only when we impose in simulations a huge helical deformation ($B_h/B_{0,0} = 75\%$), which is a rather unrealistic case for the RFP. This result strengthens the perspectives of the helical RFP as a fusion configuration, and extends neoclassical theory into a new and qualitatively different magnetic regime. Besides, trapped particle orbits have relevance in astrophysics, such as in solar loops [14].

To analyze the RFX magnetic topology, particle trajectories, and associated transport, we make use of the Hamiltonian guiding center code ORBIT [15]. Equilibrium and perturbations are calculated by solving the Newcomb's equations in toroidal geometry [16], with fixed boundary conditions given by the experimental pick-up coil spectra at the wall, $\delta B(\psi_p, \theta, \zeta) = \sum_{m,n} B_{m,n}(\psi_p) \sin(m\theta - n\zeta)$ (with m, n the poloidal and toroidal mode numbers, and θ, ζ the corresponding angles). In this way, the pure single helicity (SH) state corresponds to a single harmonic $m = 1$, $n = 7$; the QSH state (with and without separatrix [9], double- and single-axis, DAx and SHAx, respectively) is obtained with a small but finite residual chaos due to the $m = 1$, $n > 7$ modes, and finally, the chaotic MH state corresponds to a broad $m = 1$ spectrum. An example of a transition from MH to DAx and SHAx is shown in Fig. 1. Contrary to MH, the DAx and, even more, the SHAx states display a region of conserved helical flux surfaces [see the

seven islands in the toroidal Poincaré plot of Figs. 1(e) and 1(f)], corresponding to an internal transport barrier with steep electron temperature gradients (up to 4–5 keV/m [17]). SHAx states share a complex 3D geometry with stellarators, but, unlike stellarators, RFPs are self-organized, low β plasmas [8] with a safety factor q monotonically decreasing from the core ($q \approx 0.12$) to the edge [$q \approx 0$, see Fig. 2(a)]. The SHAx is a result of currents flowing in the plasma; thus, the effective helical ripple ϵ_h is also large in the core and small in the edge [Fig. 2(a), dashed line]. This sets a difference with stellarators, characterized by $q \sim 1$ and a helical field generated by external coils, with large edge ϵ_h [12,13].

To calculate D in the three different magnetic topologies of Fig. 1 we evaluate the steady state distributions $n(\psi_p)$ by fixing source and sink in a fixed domain [18]. Lost particles are reinserted at the center with uniform pitch (= normalized parallel velocity $\lambda = v_\parallel/v$). Particles are 1000 H^+ ions with energy $E = 400$, 750 and 900 eV in MH, DAx and SHAx, respectively. In the SHAx state the domain has been modified to match the helical flux surfaces [19]. While in MH the domain covers a few Larmor radii, in SHAx and/or DAx the domain covers the whole helical core, so that D in this case has to be intended as a volume average. We limit our discussion to ion dynamics, the study of electron diffusion and associated ambipolar electric field are ongoing work, but initial results do not show significant ambipolar corrections to the ion D [19].

The core of our analyses consists in studying the resulting D as a function of the collision frequency per toroidal transit time, $\nu\tau_{\rm tor}$ ($\tau_{\rm tor} = 2\pi R_0/v_{\rm th}$ with $v_{\rm th}$ the thermal velocity and R_0 the major radius). The results are shown in Fig. 2(b). At low collisions $D^{\rm SHAx} < D^{\rm DAx} \ll D_{mh}$, virtually neoclassical: the shaded regions correspond to the typical H^+ ion collisionality ranges found in experimental QSH and MH states. The larger $D^{\rm DAx}$ is consistent with residual chaos which is found in the vicinity of the separatrix in the transition from QSH to MH, while in the fully chaotic state the inverse dependence on collisions is expected in transport dominated by Lévy flights [18,20]. Our main point is that $D^{\rm SHAx} \propto \nu$ consistent with a banana-dominated (BN) transport [13], therefore not showing the $1/\nu$ behavior typical of the superbanana (SB) branch [see Fig. 2(c)]. It is worth mentioning that the magnitude of $D^{\rm SHAx}$ is not much larger than the classical value $D^{\rm cl}$, since in the RFP the small q limits the banana width to a few mm [18,19]: in this way, the issue of neoclassical effects on transport is *a priori* less stringent in the RFP than in stellarators or tokamaks.

The transition from banana to plateau happens at $\nu\tau_{\rm tor} \sim 0.1$. Translating this value to the normalized collision frequency used in stellarator theory, $\nu^\star = \frac{R}{r}\frac{\nu}{\omega_b} = \frac{\sqrt{2}qR}{\epsilon^{3/2}v_{\rm th}}\nu$, with ω_b the maximum bounce frequency and $\epsilon = r/R$, the transition is found at $\nu^\star = 0.04 \simeq 2/n^2 = 2\iota^2$, typical of a helically symmetric system with $n = 7$ turns [13]. Since this value of $\nu^\star$ is relatively low, the transition from PL to the PS regime happens at comparatively lower collisionality than in most stellarators ($\nu\tau_{\rm tor} > 10$). In the PS regime particles are not able to experience the details of the magnetic topology. As a consequence, transport is rather undifferentiated in MH, DAx and SHAx (D_{mh} is slightly lower due to lower ion energy in MH). Indications in this direction are given by laser blow-off experiments with nickel targets in RFX-mod [21]. ORBIT runs with Ni^{7+} ions confirm this picture, since for this species $\nu\tau_{\rm tor} \sim 10$.

The results shown in Fig. 2 for RFP transport should be compared to other helical devices: in stellarators, particles trapped in the helical ripple acquire nonzero bounce-averaged radial drifts when a helix is bound into a torus [13]. This mechanism is essentially collisionless, since helically trapped (superbanana) particles can exit the system in between one collision and the next, giving as a result $D_{\rm sb} \propto 1/\nu$. A natural question is why this mechanism is not seen in the helical RFP.

An initial clue is given by the statistical analysis of particles lost during the SHAx run: this is shown in Fig. 3, which displays the test particle pitch distribution at the beginning [panel (a)] and end [panel (b)] of the run. While the initial pitch distribution is flat, the final distribution has rather strong tails towards high λ, namely, at the

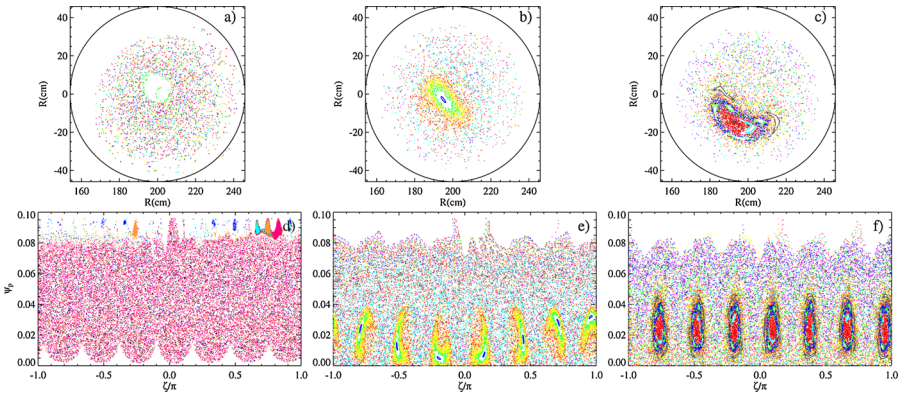

FIG. 1 (color online). (a)–(c) Poincaré plots on the poloidal section for a MH [discharge #23977, $t = 24$ ms, (a)], DAx [# 21982, $t = 125$ ms, (b)] and SHAx [#23977, $t = 174$ ms, (c)] state; (d)–(f) corresponding toroidal sections.

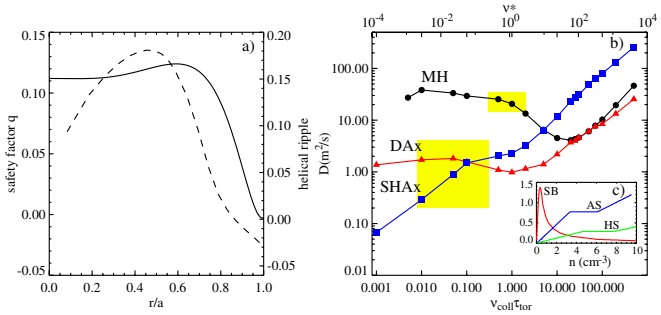

FIG. 2 (color online). (a) Safety factor (solid line) and helical ripple (dashed line) profiles in RFX-mod; (b) Diffusion coefficient D of H^+ ions as a function of $\nu\tau_{tor}$, MH (black circles), DAx (red triangles), SHAx (blue squares) and [inset, (c)] schematic view of the neoclassical transport regimes: AS = axisymmetric system, HS = helically symmetric, SB = superbanana (adapted from Ref. [13]).

end of the run there is a consistent population of passing particles, which, in addition to this, are found at the boundary of the helical domain [Fig. 3(c)]. This means that particles that (possibly) start as superbananas end up being passing, since the plasma is axisymmetric outside the helical structure [$q \sim 0$ and $\epsilon_h \sim 0$, Fig. 2(a)], and passing particles experience very low transport in QSH [19].

To verify his hypothesis, we launched ~8000 particles, no collisions, and we looked directly at the orbits in two situations: the pure SH with $B_h/B = 10\%$, and an artificial helical SH state with $B_h = 7.5$ times the natural amplitude ($B_h/B = 75\%$). The initial conditions cover the whole helical domain on a poloidal section, $0.1 < \frac{\psi_p}{\psi_{p,w}} < 0.85$ and $-\pi < \theta < \pi$, $\psi_{p,w}$ being the poloidal flux at the wall. For each initial condition ($\psi_p^{(i)}$, $\theta^{(j)}$) we varied the initial pitch in the range $0.01 < \lambda < 1$ and calculated the critical pitch λ_c that separates trapped ($\lambda < \lambda_c$) and passing ($\lambda > \lambda_c$) particles (for passing particles the pitch has a constant sign). Among the trapped population, we extracted the subset corresponding to superbananas by analyzing the motion in the toroidal angle. In fact, ordinary bananas experience a motion which is bounded poloidally ($-\theta_b < \theta < \theta_b$) and unbounded toroidally with a

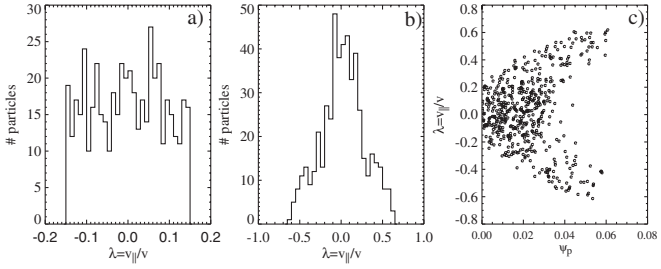

FIG. 3. (a) Density distribution of deposited particles, as a function of the pitch $\lambda = v_\parallel/v$; (b) the same, at the end of the run; (c) pitch as a function of the flux coordinate ψ_p, showing that lost particles are mostly passing.

precession rate $\omega_d \simeq Eq/(mrR\omega_0)$, E being the particle energy and ω_0 the cyclotron frequency [2]. On the contrary, superbananas are bounded toroidally ($-\zeta_b < \zeta < \zeta_b$) and unbounded poloidally, since they are trapped in the helical ripple. We finally defined the exit time τ_{loss} as $\psi_p(\tau_{loss}) = \psi_{p,w}$. If $\tau_{loss} \ll$ run time, then the particle is able to exit without collisions.

Let us start with the artificially large helical state: Fig. 4(a) shows a contour plot of the critical pitch on the poloidal plane. The average critical pitch $\langle\lambda_c\rangle = 0.4$, which is 30% larger than the axisymmetric case with no helical field, $\langle\lambda_{c,0}\rangle = 0.3$. The distribution $\lambda_c(r, \theta)$ shows a prominent accumulation of trapped particles in the outboard side of the helical contour (where $\lambda_c \sim 0.7$), all the way up to the boundary, where the helical ripple is large: in the same region the superbananas amount to ~100% of trapped particles [Fig. 4(b)]. The superbananas can exit the system in a rather short time [Fig. 4(c)]. The inner half of the helix on the contrary contains ordinary bananas with no appreciable radial drifts; they finish the run without being lost. The percentage of superbananas is ~30% of the total number of particles. Finally, we checked the criterion used to tag the superbananas: in fact, when τ_{loss} is short, it is difficult to distinguish a superbanana from a slowly preceding banana. In an axisymmetric system the toroidal canonical momentum in the guiding center equations of motion, $P_\zeta = g\rho_\parallel - \psi_p$, is conserved [2]: the banana trajectory is therefore a closed orbit with a definite separatrix. In a helical system P_ζ is not conserved, banana

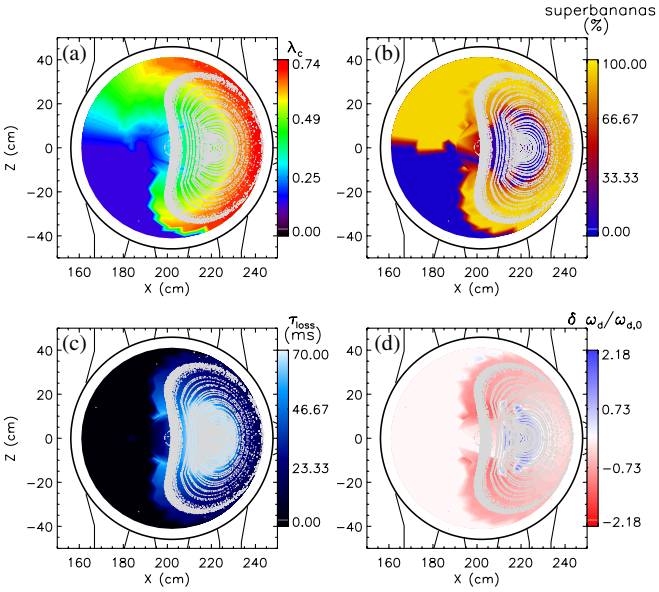

FIG. 4 (color online). (a) Critical pitch λ_c plotted on the poloidal section, in a case with a helical deformation 7.5 times the experimental value; (b) percentage of superbananas over the trapped population; (c) escape time of particles (runtime ~70 ms); (d) variation of the toroidal precession rate with respect to the unperturbed case, $\delta\omega_d/\omega_d$. In all panels, the Poincaré plot of the island is overplotted to the color contours.

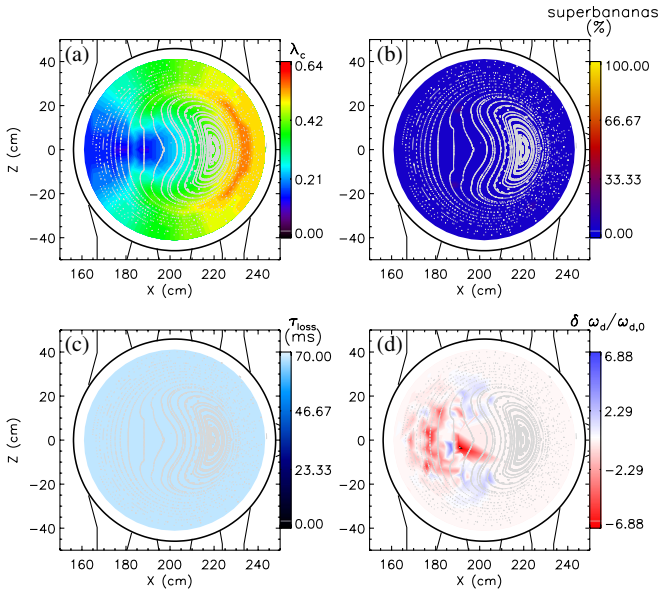

FIG. 5 (color online). (a) Critical pitch λ_c plotted on the poloidal section, in the experimental case; (b) percentage of superbananas over the trapped population; (c) escape time of particles (runtime ~70 ms); (d) variation of the toroidal precession rate with respect to the unperturbed case, $\delta\omega_d/\omega_d$.

orbits are not closed, and the banana-superbanana boundary is not well defined. Nevertheless, superbanana particles possess very low toroidal precession rates. By comparing this rate with the unperturbed ($B_h = 0$) value, $\delta\omega_d/\omega_{d,0} = (\omega_d - \omega_{d,0})/\omega_{d,0}$ we can distinguish bananas ($\delta\omega_d/\omega_{d,0} \gg 1$) and superbananas ($\delta\omega_d/\omega_{d,0} \ll 1$). Figure 4(d) shows a contour plot of $\delta\omega_d/\omega_{d,0}$, and by comparing to Fig. 4(b) we conclude that particles tagged as superbananas have very low ω_d, as expected.

Let us now turn back to the realistic situation ($B_h/B = 10\%$): Fig. 5(a) shows the $\lambda_c(r,\theta)$ distribution (average $\langle\lambda_c\rangle = 0.38$). There is a local radial increase of the trapped fraction at the edge of the helical domain (where $\lambda_c \sim 0.6$), as already pointed out in the RFX [22], but then at larger radii λ_c falls down to 0.3–0.4. This fact explains the behavior of Fig. 3: a particle that starts its trajectory below threshold at the edge of the helix, drifting outwards it can become passing due to the rapid decrease of the critical pitch. The dominant mechanisms at this level of B_h are the lack of superbanana trajectories [Fig. 5(b)], associated collisionless losses [Fig. 5(c)], and negligible perturbation of the toroidal precession rate in the island region [Fig. 5(d)]. Lacking superbanana losses, the SHAx RFP cannot show any dependence of the type $D_{sb} \sim 1/\nu$ at low collisionalities.

Summarizing, a test particle evaluation of the diffusion coefficient in the RFX-mod RFP shows a decrease of transport in the transition from MH to QSH, up to neoclassical values. In the helical SHAx state the RFP recovers the usual collisional dependence of transport in tokamaks and stellarators (banana, plateau, and Pfirsch-Schlüter). In addition to this, the almost total absence of helically trapped (superbanana) particles at the levels of helical deformation seen in experiment ($B_h/B = 10\%$) excludes the presence of the superbanana $1/\nu$ branch typical of unoptimized stellarators. Besides, the transition from banana to plateau happens at $\nu^\star \simeq 2\iota^2$, therefore at rather low collisionality. The consequence is that even light impurities, such as carbon or oxygen, are likely to be in the fully collisional, Pfirsch-Schlüter regime, with associated problems of high transport and edge accumulation.

We acknowledge discussions with Dr. Shichong Guo, who first in RFX raised the issue of the collisional dependence of RFP transport, and Dr. Lorella Carraro for stimulating the impurity study.

*marco.gobbin@igi.cnr.it
†gianluca.spizzo@igi.cnr.it

[1] E. J. Doyle (Chair Transport Physics) *et al.*, Nucl. Fusion **47**, S18 (2007).
[2] R. B. White, *The Theory of Toroidally Confined Plasmas* (Imperial College Press, Covent Garden, London UK, 2006), 2nd ed..
[3] A. J. Lichtenberg and M. A. Lieberman, *Regular and Chaotic Dynamics* (Springer-Verlag, New York, USA, 1992), 2nd ed., p. 428.
[4] M. Wakatani and R. Itatani, J. Phys. Soc. Jpn. **34**, 181 (1973).
[5] A. B. Rechester and M. N. Rosenbluth, Phys. Rev. Lett. **40**, 38 (1978).
[6] K. H. Spatschek, AIP Conf. Proc. **1013**, 250 (2008).
[7] G. Zimbardo, P. Veltri, and P. Pommois, Phys. Rev. E **61**, 1940 (2000).
[8] S. Cappello *et al.*, AIP Conf. Proc. **1069**, 27 (2008).
[9] R. Lorenzini *et al.*, Nature Phys. **5**, 570 (2009); D. F. Escande *et al.*, Phys. Rev. Lett. **85**, 3169 (2000).
[10] P. Sonato *et al.*, Fusion Eng. Des. **66–68**, 161 (2003).
[11] L. Marrelli *et al.*, Plasma Phys. Controlled Fusion **49**, B359 (2007).
[12] G. Grieger *et al.* (W7-X Team and W7-AS Team), Phys. Fluids B **4**, 2081 (1992).
[13] H. E. Mynick, Phys. Plasmas **13**, 058102 (2006).
[14] M. Gkioulidou, G. Zimbardo, P. Pommois, P. Veltri, and L. Vlahos, Astronomy & Astrophysics **462**, 1113 (2007).
[15] R. B. White and M. S. Chance, Phys. Fluids **27**, 2455 (1984).
[16] P. Zanca and D. Terranova, Plasma Phys. Controlled Fusion **46**, 1115 (2004).
[17] M. E. Puiatti*et al.*, Plasma Phys. Controlled Fusion **51**, 124031 (2009).
[18] G. Spizzo, R. B. White, S. Cappello, and L. Marrelli, Plasma Phys. Controlled Fusion **51**, 124026 (2009).
[19] M. Gobbin, L. Marrelli, and R. B. White, Plasma Phys. Controlled Fusion **51**, 065010 (2009).
[20] D. del Castillo-Negrete, AIP Conf. Proc. **1013**, 207 (2008).
[21] L. Carraro *et al.*, Nucl. Fusion **49**, 055009 (2009).
[22] I. Predebon, L. Marrelli, R. B. White, and P. Martin, Phys. Rev. Lett. **93**, 145001 (2004).